Dynamics of lock-release gravity currents over sparse and dense rough bottoms

Claudia Cenedese[1], Roger Nokes[2] and Jason Hyatt[3]

[1]Department of Physical Oceanography, Woods Hole Oceanographic Institution
ccenedese@whoi.edu

[2] Department of Civil and Natural Resources Engineering, University of Canterbury

[3] Department of Science and Mathematics, Massachusetts Maritime Academy

Abstract

Dense oceanic overflows mix with surrounding waters along the descent down the continental slope. The existing parameterizations for entrainment in dense currents account primarily for the shear-induced entrainment at the interface between the dense flow and the ambient fluid. However, the turbulence generated by roughness elements at the bottom boundary, which produces an enhanced drag, can be intense and must be considered. This paper describes an experimental study investigating the dynamics of a lock-release dense gravity current propagating through 'sparse' and 'dense' bottom roughnesses. Two main regimes are observed in which the entrainment/dilution of the current is enhanced due to different mechanisms. For the sparse configuration the dense current is observed to propagate between the roughness elements while for the dense configuration it rides on top of the cylinders.

1 Introduction

The amount of mixing and entrainment at the interface of the dense currents dictates the final properties of these overflows, and thus is of fundamental importance to the understanding of the formation of deep water masses. Oceanographic measurements through dense currents suggest that the top of the current is usually characterized by a large velocity shear, low Richardson number and large turbulent displacements indicative of entrainment due to shear-driven mixing (Peters and Johns, 2005). Low Richardson number are also observed near the bottom of the dense current due to the large shear caused by frictional drag.

Although several studies have investigated entrainment in dense currents and proposed improved parameterizations (Hallberg 2000; Xu et al. 2006; Jackson et al. 2008; Cenedese and Adduce 2010), the main focus has been on the shear-induced entrainment at the interface between the dense flow and the ambient fluid. Comparatively little work has been done on the entrainment and dilution due to roughness elements at the bottom boundary.

A closely related topic that has been investigated recently is fluid flow through aquatic canopies of various types and Nepf (2012) provides an overview of the research in the area. In particular, Zhang and Nepf (2011) focused on the dynamics of a surface gravity current propagating through a suspended canopy generated by an array of circular cylinders using an experimental PIV system.

This paper describes part of a larger investigation into the dynamics of lock-release gravity

currents over rough bottoms. In particular, we focus on the impact of different spacing between the roughness elements and different height of the elements on the dynamics regulating the gravity current entrainment and dilution.

2 Methods

2.1 Experimental Apparatus

Experiments were conducted in a similar set up to that described in Nokes et al. (2016). The tank was $L_T = 620$ cm long, $H_T = 50$ cm high and $W_T = 25$ cm wide with a flat bottom, as illustrated in figure 1. The classic lock exchange configuration was employed to generate a dense gravity current. A stainless steel gate, sealed by plastic foam, divided the tank into two regions where the dense and lighter fluids were located. The dense fluid region was 100 cm long while the roughness elements were located in the lighter fluid region for 300 cm behind the gate (figure 1).

The roughness elements consisted of rigid plastic cylinders with a diameter of $d = 2$ cm and height that was varied between $h = 1$, 2, or 5 cm. The cylinders were screwed into an aluminum base plate and could be removed or added to produce varying roughness configurations. The spacing of the cylinders was varied to obtain the two configurations illustrated in figure 2. In the sparse and dense configurations the distance between the centers of the cylinders was $\Delta S = 3.2$ cm and 6.4 cm, respectively.

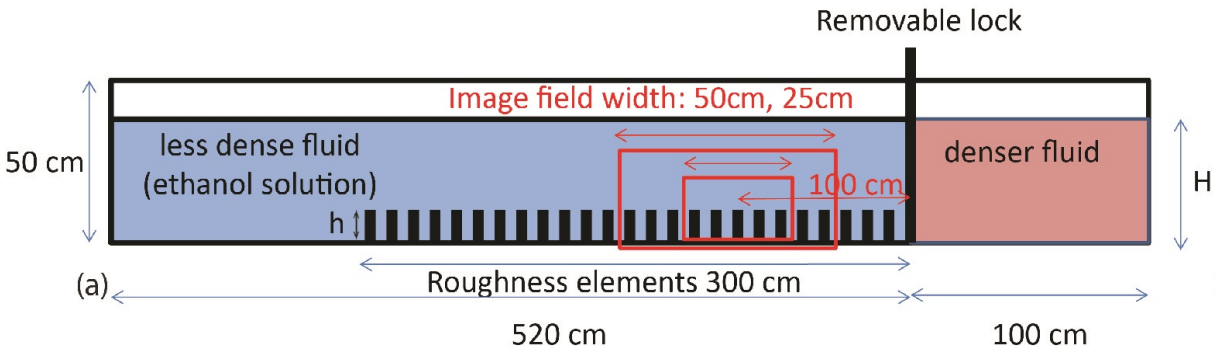

Figure 1: Schematic of the experimental apparatus, side view. Not to scale.

The density difference between the current and the ambient fluid $\Delta\rho$ produced a reduced gravity $g' = g\Delta\rho/\rho = 5$ cm/s^2 for all experiments. In order to obtain this $\Delta\rho$ and avoid refraction of light while the fluids moved through or above the cylinders, the indices of refraction of the dense and light fluids were matched ($n = 1.3336$) by adding salt to the dense water (4 g/l, $\rho \approx 1.0014$ g/ml) and clear denatured ethanol to the light water (14 ml ethanol per 114 ml ethanol water mixture, $\rho \approx 0.9963$ g/ml). The densities of the two fluids were measured with an Anton Parr DMA5000 density meter. The depth of the fluid in the tank H took values of 35, 27, 20, 15 and 10 cm to obtain a range of values for non-dimensional number associated with the flow's initial condition

$$\lambda = \frac{h}{H}, \tag{1}$$

which is the ratio of the cylinder height to the water depth. In the present experiments λ varied between 0.03 and 0.5.

As in Nokes et al. (2016), three independent dimensionless parameters characterize the bottom roughness.The plan density, σ, defined by

$$\sigma = \frac{A_P}{A_{TP}}, \tag{2}$$

where A_P is the area of the base covered by the cylinders in plan and A_{TP} is the total area of the base in plan; μ, the elevation density, defined by

$$\mu = \frac{A_E}{A_{TE}}, \tag{3}$$

where A_E is the area of the field covered by the cylinders in elevation as seen by the advancing current and A_{TE} is the total area of the field in elevation (measured to the top of the cylinders); and α, the aspect ratio, defined by

$$\alpha = \frac{h}{d}. \tag{4}$$

In the present experiments the above roughness parameters took the values of $\sigma = 0.09$ and $\mu = 0.31$ for the sparse configuration and $\sigma = 0.35$ and $\mu = 0.62$ for the dense configuration. The value of α took the values 0.5, 1 and 2.5 for each configuration.

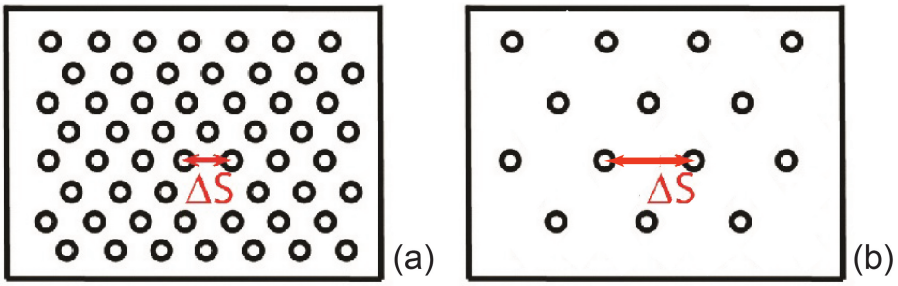

Figure 2: Top view of the cylinders representing the bottom roughness. (a) Dense configuration with $\sigma = 0.35$ and $\mu = 0.62$; (b) sparse configuration with $\sigma = 0.09$ and $\mu = 0.31$. Not to scale.

2.2 Density field measurements

The experiments were recorded using a JAI BB141GE video camera with a zoom lens operating at 30.13Hz. The 1392x1040 pixel images were transferred directly to a fast hard drive on a PC during capture. The camera viewed the flow through an angled mirror to extend the light path and minimize parallax. The image field of the camera was centered 100 cm downstream of the gate and was 50 cm wide. The height of the image field always contained the entire dense current.

The density field was determined using a light attenuation (LA) technique (Cenedese and Dalziel, 1998). The flow was illuminated from the rear by a bank of fluorescent bulbs. Care was taken to ensure consistent lighting throughout the calibration and experiments. A reserve of concentrated dyed red salty solution was made and the tank and lighting were calibrated by measuring density and light attenuation for 8 different dye concentrations. The concentrate was then used to create the dense fluid in the lock. The experimental densities were calculated using a calibration curve based on Beer's Law and the ratio of

the average of blue and green/red intensity. The analysis of the images was done with the Streams software, (Nokes 2016).

The final output from the LA analysis processes were non-dimensional 2D concentration fields translated into the frame of reference moving with the gravity current front. The variables were nondimensionalised as follows:

$$x' = \frac{x}{H} \qquad \text{and} \qquad y' = \frac{y}{H}, \tag{5}$$

and

$$\rho' = \frac{\rho - \rho_0}{\rho_d - \rho_0}, \tag{6}$$

where x and y are the horizontal and vertical coordinates, respectively, where the origin of y is the flume bed and the origin of x is selected to be the location of the $\rho' = 0.02$ contour near the bottom. The Froude and Reynolds numbers of the flow were defined as

$$Fr = \frac{U_f}{\sqrt{g'H}} \qquad \text{and} \qquad Re = \frac{U_f H}{\nu}, \tag{7}$$

where U_f is the front speed. In the present experiments they varied between $Fr = 0.15 - 0.47$ and $Re = 1100 - 22000$.

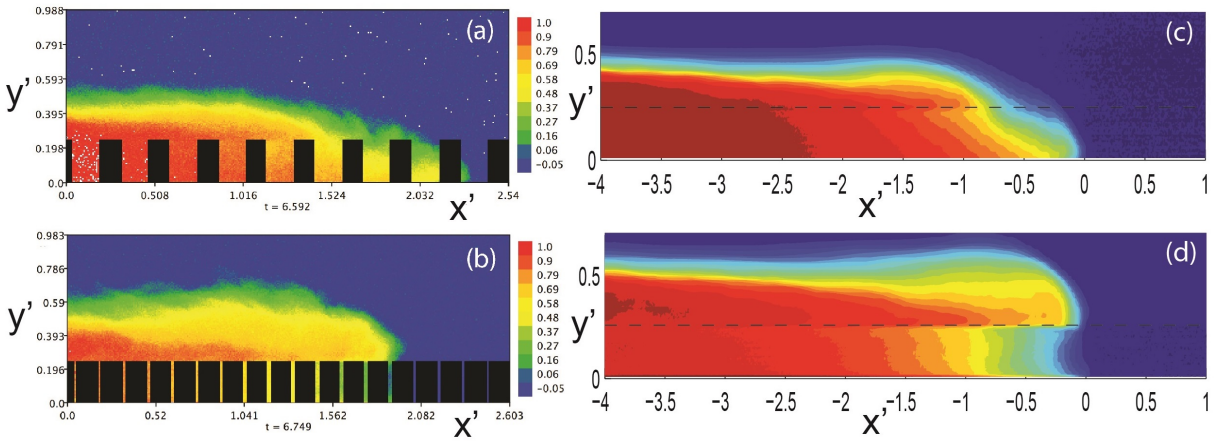

Figure 3: Instantaneous non-dimensional density filed for a gravity current propagating into a (a) sparse and (b) dense array of cylinders representing the bottom roughness. Time averaged non-dimensional density field translated into the frame of reference moving with the gravity current front for the (c) sparse and (d) dense configurations. Black dashed lines in (c) and (d) represent the height of the cylinders. The non-dimensional parameters for (a) and (c) are: $\sigma = 0.09$, $\mu = 0.31$, $\alpha = 2.5$, $\lambda = 0.25$, $Fr = 0.35$ and $Re = 7165$; and for (b) and (d) are: $\sigma = 0.35$, $\mu = 0.62$, $\alpha = 2.5$, $\lambda = 0.25$, $Fr = 0.28$ and $Re = 5600$.

3 Experimental Results

One may expect that for dense currents having a height much larger than the roughness height, the turbulent eddies generated by the bottom roughness will play a role in homogenizing the dense current but will not contribute to entrainment of ambient waters within the dense current (i.e. will not contribute to changes in the water properties). Conversely, one may expect that for dense currents having a height comparable to, or

smaller than, the roughness height, more complex regimes may occur where the turbulent eddies generated near the bottom may impact the entrainment of ambient waters and may significantly influence the dense water properties. Experimental results suggest that the above mechanisms are at play when the current propagates through the sparse array of cylinders, but a dynamically different regime occurs for the dense configuration.

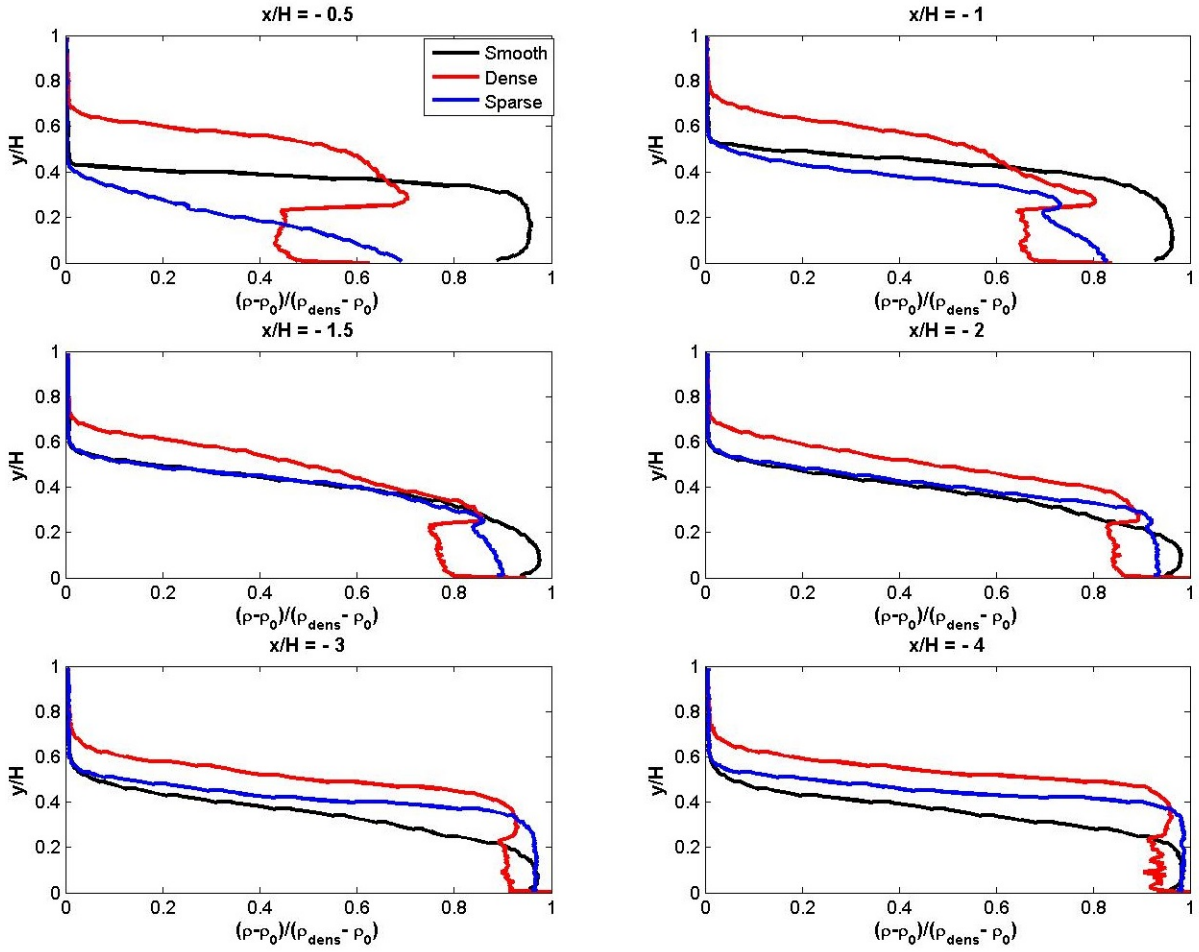

Figure 4: Time averaged non-dimensional vertical density profiles for a gravity current propagating over a smooth bottom (black) and into a sparse (blue) and dense (red) array of cylinders representing the bottom roughness. The blue and red lines are obtained from the density data showed in figure 3c and d, respectively. The non-dimensional parameters for the sparse and dense configuration experiments are the same as in figure 3 and for the smooth bottom experiment are: $\sigma = 0$, $\mu = 0$, $\alpha = 0$, $\lambda = 0$, $Fr = 0.46$ and $Re = 9313$. Different panels corresponds to different locations behind the front as indicated above the panels by $x' = x/H$.

For the sparse configuration the dense current propagates between the cylinders and the entrainment is enhanced by the vortices generated in the wake of the cylindrical obstacles, as illustrated by the instantaneous density field in figure 3a. The time averaged density field translated into the frame of reference moving with the front (figure 3c) suggests that the enhanced entrainment affects the current near the front where the density is strongly reduced when compared to that of a current propagating over a smooth bottom (blue and black lines, figure 4). With increasing distance from the front, i.e. larger $x' = x/H$, the difference in density between the smooth and sparse experiments is reduced and at $x' = 4$ the density in the two currents is almost identical, the only difference being the

larger height of the current in the sparse configuration due to the volume occupied by the cylinders.

For the dense configuration the dense current rides on top of the cylinders and the dilution is enhanced by the onset of convective instability between the dense current above the cylinders and the ambient lighter water between the cylinders (figure 3b). The convective instability proves to be an extremely efficient mechanism for diluting the dense gravity current, as illustrated by the time averaged density field in figure 3d. The density of the current is greatly reduced compared to both a gravity current in a sparse configuration and over a smooth bottom (figure 4). As for the sparse configuration, the difference in density between the dense and sparse (or smooth) experiments is reduced with increasing distance from the front, but for a dense configuration the density in the current is always lower then for a smooth case, even for large distances, e.g. $x' = 4$.

As expected, for low values of the parameter λ the dense current behavior approaches that of a current over a smooth bottom, while the largest deviations from the smooth bottom case are observed for large values of λ.

4 Conclusions

Laboratory experiments investigated the impact of bottom roughness on the dynamics regulating the entrainment and dilution of a lock-release dense gravity current. In a dense configuration with $\sigma = 0.35$ and $\mu = 0.62$ the dense current is observed to propagate on top of the cylinders and enhanced dilution of the current is generated by the onset of convective instability due to dense water being located above lighter water. In the sparse configuration with $\sigma = 0.09$ and $\mu = 0.31$ the dense current propagates between the array of cylinders and dilution near the front is enhanced by the vortices generated in the wake of the cylindrical obstacles.

References

Cenedese, C. and Adduce, C. (2010). A new parameterization for entrainment in overflows. *J. Phys. Oceanogr.*, 40:1835-1850.

Cenedese, C. and Dalziel, S. B. (1998). Concentration and depth fields determined by the light transmitted through a dyed solution. *Proceedings of the 8th International Symposium on Flow Visualization, ed. Carlomagno and Grant.* ISBN 0 953399109, paper 061.

Hallberg, R. W. (2000). Time integration of diapycnal diffusion and Richardson number-dependent mixing in isopycnal coordinate ocean models. *Mon. Wea. Rev.*, 128:1402-1419.

Jackson, L., Hallberg,R. W. and Legg, S. (2008). A parameterization of shear-driven turbulence for ocean climate models. *J. Phys. Oceanogr.*, 38:1033-1053.

Nepf, H. (2012). Flow and transport in regions with aquatic vegetation. *Annual Review of Fluid Mechanics*, 44:123-142.

Nokes, R. (2016). Streams 2.05 - System Theory and Design, University of Canterbury

Nokes, R., Cenedese, C., Ball, M. and Williams, T. (2016). The Front Condition for Gravity Currents Propagating over Rough Boundaries, VIIIth ISSF, San Diego, 2016.

Peters, H. and Johns,W. E. (2005). Mixing and entrainment in the Red Sea outflow plume. Part II: Turbulence characteristics. *J. Phys. Oceanogr.*, 35:584-600.

Xu, X., Chang,Y. S., Peters, H., Ozgokmen, T. M. and Chassignet, E. P. (2006). Parameterization of gravity current entrainment for ocean circulation models using a high-order 3D nonhydrostatic spectral element model. *Ocean Modell.*, 14:19-44.

Zhang, X. and Nepf, H. (2011). Exchange flow between open water and floating vegetation. *Environmental Fluid Mechanics*, 11:531-546.